Sensors and Actuators B 252 (2017) 62–71

Contents lists available at ScienceDirect

Sensors and Actuators B: Chemical

journal homepage: www.elsevier.com/locate/snb

Electrochemical aptasensing of human cardiac troponin I based on an array of gold nanodumbbells-Applied to early detection of myocardial infarction

M. Negahdary[a,b], M. Behjati-Ardakani[a], N. Sattarahmady[b,c], H. Yadegari[d], H. Heli[b,*]

[a] Yazd Cardiovascular Research Center, Shahid Sadoughi University of Medical Sciences, Yazd, Iran
[b] Nanomedicine and Nanobiology Research Center, Shiraz University of Medical Sciences, Shiraz, Iran
[c] Department of Medical Physics, School of Medicine, Shiraz University of Medical Sciences, Shiraz, Iran
[d] Department of Mechanical and Materials Engineering, University of Western Ontario, London, Ontario N6A 5B9, Canada

ARTICLE INFO

Article history:
Received 9 March 2017
Received in revised form 22 May 2017
Accepted 24 May 2017
Available online 30 May 2017

Keywords:
Aptasensor
Myocardial infarction
Troponin I
Biomarker
Electrochemical biosensor

ABSTRACT

Recently, convergence of nanotechnology, medicine, biology and chemistry has provided novel solutions for efficient diagnosis systems for disease markers. A detection method of troponin I (TnI), as the gold standard of acute myocardial infarction biomarker, was investigated and a novel aptasensor was presented for this biomarker. An array of gold nanodumbbells was firstly synthesized using putrescine as the shape directing agent at a surface. It was then applied as a transducer for the immobilization of a 76-mer TnI aptamer to fabricate a simple electrochemical TnI aptasensor. Using the aptasensor, TnI was detected in a linear range of 0.05–500 ng mL^{-1} with a limit of detection of 8.0 pg mL^{-1}. The aptasensor showed a diagnostic sensitivity of 100% and a diagnostic specificity of 85% when challenged with blood serum samples of 89 individuals.

1. Introduction

Heart diseases are considered as the most common cause of death in most countries in the world and are the main leading cause of disability [1]. Blocked heart blood vessels can inhibit blood circulation in heart and can leading to blood clots in the heart's arteries and acute myocardial infarctions (AMIs) in peoples [2]. If medical aids do not timely found by these patients, the heart's muscles will undergo irreversible damages [3] due to inability of absorption of enough oxygen. AMI is occurred due to the lack of oxygen in different parts of the heart and all of the heart's areas will be in oxygen deficiency [4]. AMIs can cause to death (11.8% of all deaths in the world [5]), otherwise, the patients suffer from heart failure, shortness of breath, swelling of legs, early fatigue and other symptoms such as a rapid heartbeat during activity and rest [6]. Therefore, rapid and precise diagnosis of AMIs is very important [7]. On the other hand, the symptoms of AMI in most cases are confused with the stomach gastritis disease, and this issue is considered also as a challenge to accurate AMI identification. Due to the high mortality and importance of prevention for serious complications after an AMI, early detection and treatment is inevitable [8].

Recently the relationship between cardiac myocytes damages and increased levels of cardiac biomarkers has been discovered [9]. For example, after an AMI, a biomarker troponin is released from damaged cardiac myocytes into bloodstream [10], and the most important laboratory test for detecting AMI is based on the troponin assay as a preferred biomarker. Troponin complex consists three subunits of troponin C (TnC), troponin T (TnT) and troponin I (TnI). They along with tropomyosin are located on actin filaments and their existence is essential in heart and skeletal muscle contraction systems mediated by calcium [11]. Cardiac TnC is not specific for heart, and is not employed for the AMIs diagnosis. Cardiac TnI is more specific for heart muscle than TnT, is not observed in skeletal muscles, does not affect against kidney disease (false positive) [8,12], and is considered as the "gold standard" for the diagnosis of myocardial injury [13].

Up to now, detection of cardiac disease biomarkers has been performed by a variety of methods of surface plasmon resonance [14,15], capacitive sensing [16,17], fluorescence immunochromatography [18], field-effect transistor [19], electrochemistry [20,21], electrogenerated chemiluminescence [22–24] and immunoassay [21,25]. However, immunogenicity and high production costs, have limited their clinical utility [26]. Detection of biomarkers using biosensors (mainly aptasensors) has been followed in recent years [27,28]. Cardiac disease biomarkers of C-reactive protein [14–16,29], natriuretic peptides [30] and TnI [31]

* Corresponding author.
E-mail addresses: hheli7@yahoo.com, heli@sums.ac.ir (H. Heli).

http://dx.doi.org/10.1016/j.snb.2017.05.149
0925-4005/

have also been detected using aptamers. Aptamers have diverse advantages over antibodies including easy modification and high stability in harsh physical and chemical environments, rapid and economical production, no batch-to-batch variation, low immunogenicity and high flexibility [32]. Up to now, there is a little report on the application of aptamer in the electrochemical detection of TnI biomarker [31].

Nanotechnology has provided materials with a high real surface area with quantum confinement and small-size effects resulted in the fabrication of sensors and biosensors with a higher sensitivity and selectivity [33–36]. A variety of nanomaterials including metal nanostructures, metal oxide nanostructures, silica nanoparticles, carbonaceous nanomaterials and their composites with the unique properties of controllable physicochemical properties, high surface area, stability and biocompatibility have been employed to fabricate biosensors [33–36]. Nanostructured materials have also been conjugated with aptamers to fabricate aptasensors with different transduction methods [37–39]. For the biomarkers, different nanostructured materials have been employed to fabricate aptasensors [40,41].

In the present study, a specific aptasensor was design on an array of gold nanodumbbells and electrochemical detection was applied for accurate detection of TnI, and a quick diagnosis method for AMI detection was developed. The aptasensor was compared with ELISA method in the assay of samples from healthy persons and patients.

2. Experimental section

2.1. Materials

All chemicals were of analytical grade from Merck (Germany) or Scharlau (Spain), and were used without further purification. TnI from human heart, bilirubin, hemoglobin, human serum albumin and heparin were purchased from Sigma (USA). TnI AccuBind ELISA Kit was purchased from Monobind (USA). A 5′ end thiol-modified DNA aptamer (the aptamer) was purchased from Bioneer (Korea) with the following sequence:

5′-(SH)-$(CH_2)_6$-AGTCTCCGCTGTCCTCCCGATGCACTTGACG TATGTCTCACTTTCTTTTCATTGACATGGGATGACGCCGTGACTG-3′

2.2. Apparatus

Electrochemical measurements were performed in a conventional three-electrode cell powered by a μ-Autolab potentiostat/galvanostat (the Netherlands). An Ag/AgCl, 3 mol L^{-1} KCl, a platinum wire, and a gold disk (Au electrode, 2 mm of diameter) or the Au electrode covered with an array of gold nanodumbbells (ND-Au electrode) were employed as the reference, counter and working electrodes, respectively. The system was run on a PC by GPES 4.9 software. Screen-printed electrodes were purchased from DropSens (Spain) and employed in some experiments. Time-dependent open circuit potential (OCP) measurements were carried out by a Mastech MS8340B digital multimeter (China) connected to a PC and its software.

Field emission scanning electron microscopy (FESEM) was performed using a Zeiss, Sigma-IGMA/VP (Germany) equipped with energy-dispersive X-ray spectroscopy (EDS). The samples were coated by a 2–5-nm thin film of gold by sputtering.

2.3. Preparation of the ND-Au electrode

Firstly, the Au electrode was polished on a sand paper and then a polishing pad with 50 nm-alumina powder lubricated by water. Polishing was continued to reach a mirror-like surface. The electrode was immersed in a 1:3 water/ethanol mixture and ultrasonicated for 8 min in an ultrasound bath. The Au electrode was then placed in the synthesis solution contained 500 mmol L^{-1} H_2SO_4, 20 mmol L^{-1} $HAuCl_4$ and 150 mmol L^{-1} putrescine. Electrodeposition was performed at 0 mV for 300 s. The ND-Au electrode was then rinsed thoroughly with distilled water.

2.4. Immobilization of the aptamer

A lyophilized aptamer sample was dissolved in appropriate distilled water. Then, 10 μL dithiothreitol (DTT) solution (containing 10 mmol L^{-1} sodium acetate, pH 5.2 and 500 mmol L^{-1} DTT) was added, mixed, and incubated at room temperature for 15 min. Excess DTT and unwanted thiol fragments were removed from the

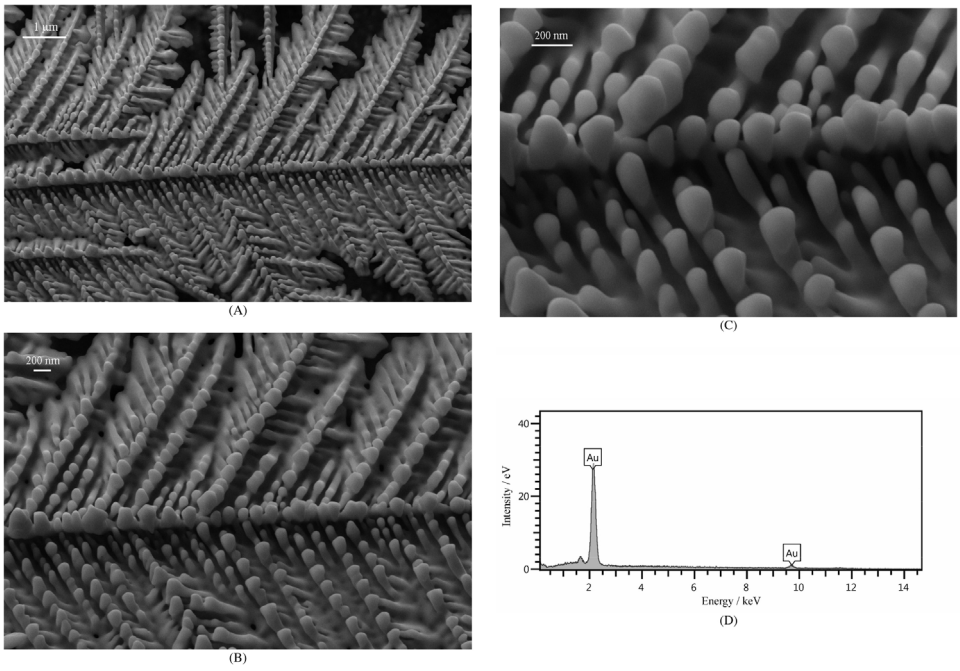

Fig 1. FESEM images (A-C) and an EDS spectrum (D) of the ND-Au electrode surface.

mixture by three times extracting with ethyl acetate (total volume of 150 μL), and the upper layer was discarded. The next step was then immediately followed because the free sulfhydryl group is unstable.

Immobilization of the aptamer on the gold surfaces was performed by dropping 10 μL of 10.0 μmol L^{-1} aptamer solution dissolved in 10 mM phosphate buffer saline containing 5 mmol L^{-1} NaCl and 2 mmol L^{-1} KCl and 1 mmol L^{-1} $MgCl_2$, pH 7.4 on the Au or ND-Au electrode surfaces and kept refrigerated at 4 °C for various times (including an optimized time of 80 min, vide infra). Then, the electrodes were rinsed with Tris-HCl buffer, 20 mM, pH 7.4 (Tris). The aptamer-modified electrodes were further treated with 1.0 mmol L^{-1} 6-mercapto-1-hexanol at room temperature for 30 min to obtain a well aligned aptamer monolayer [42,43]. Then the electrodes were washed again with Tris and double distilled water, respectively, to remove unspecific adsorbed thiols. The obtained Au- and ND-Au-modified aptamer electrodes were denoted as the Au/aptamer electrode and the aptasensor, respectively. The prepared electrodes in this step were ready to use and when not used, they were stored in Tris at 4 °C.

2.5. TnI binding to the aptamer

The binding process was performed by immersing the Au/aptamer electrode or the aptasensor into Tris containing various concentrations of TnI for 40 min at 37 °C (vide infra). Then, the aptasensor was rinsed with Tris to remove non-bonded TnI. It was then inserted in a solution of Tris + 0.5 mol L^{-1} KCl + 0.5 mmol L^{-1} ferro/ferricyanide and differential pulse voltammograms (DPVs) for the oxidation peak of ferro/ferricyanide redox couple were recorded with a pulse width of 25 mV, a pulse time of 50 ms, and a scan rate of 10 mV s^{-1}. The concentration of TnI was quantified as the ferro/ferricyanide oxidation peak current.

2.6. Electrochemical measurements

OCP measurements during the self assembling process of the aptamer on the gold nanodumbbells surface were done using an ND-Au screen-printed electrode refrigerated during the measurements. All electrochemical measurements otherwise those related to OCP measurements were performed at room temperature.

2.7. Patient samples and ELISA procedure

Blood samples (5 mL) obtained from humans (equal women and men persons) after filling a consent form by each person. The persons were referred to a clinical lab to identify AMI symptom. The values of TnI concentrations in all the samples were determined by ELISA measurements in 96-well plates coated with streptavidin. A calibration curve using standard solutions of TnI of 0, 1, 3, 6, 15 and 30 ng mL^{-1} was plotted. Then, serum was extracted from the blood samples and analyzed by the ELISA kit, according to its instruction. These samples were then diluted with distilled water (to place within the linear range of the aptasensor) and assayed by the aptasensor using a calibration curve.

3. Results and discussion

3.1. Characterization of the gold nanodumbbells

The details of preparation of the ND-Au electrode are schematically shown in Supplementary material S1. The surface morphology and size of the gold nanodumbbells were investigated by FESEM. Fig. 1 shows FESEM images (A-C) of the ND-Au electrode surface with different magnifications and an EDS spectrum (D). In the images, arrays of dumbbells of about 50–150 nm in diameter are observed covering entire the surface. The nanodumbbells have a

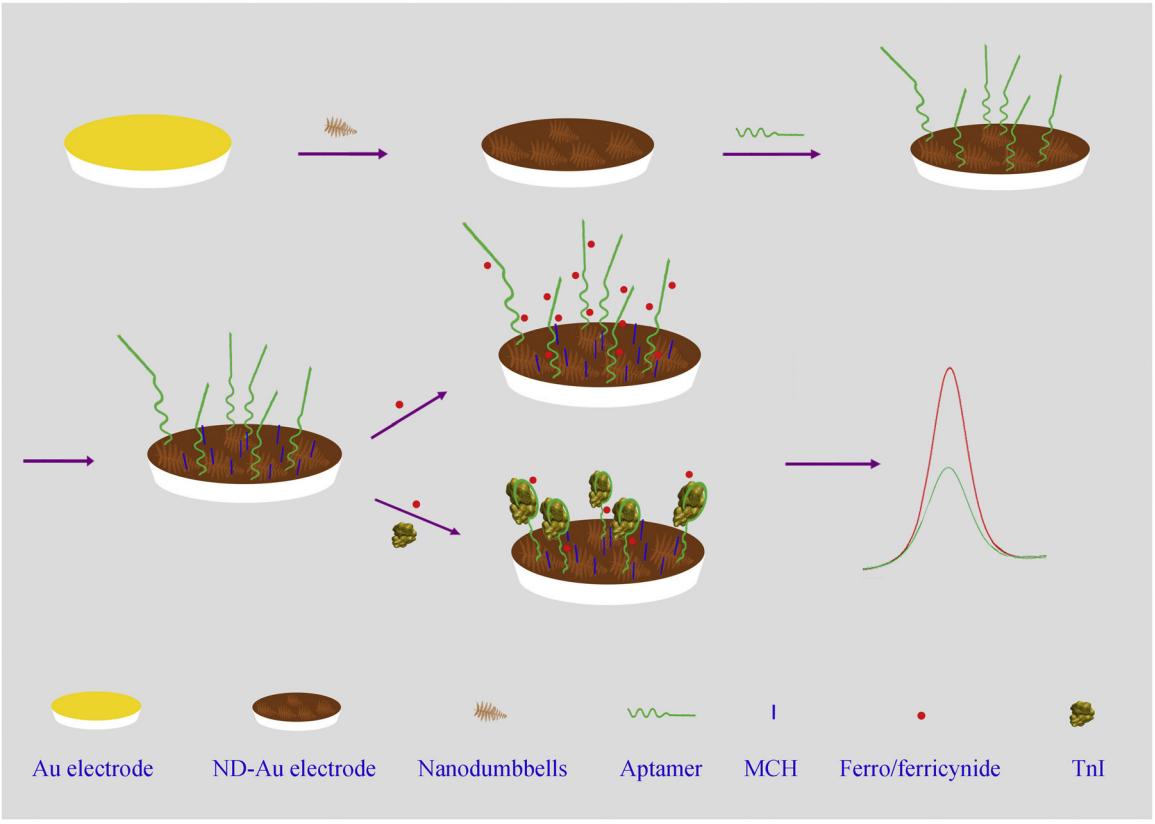

Scheme 1. Fabrication protocol of the aptasensor and TnI detection.

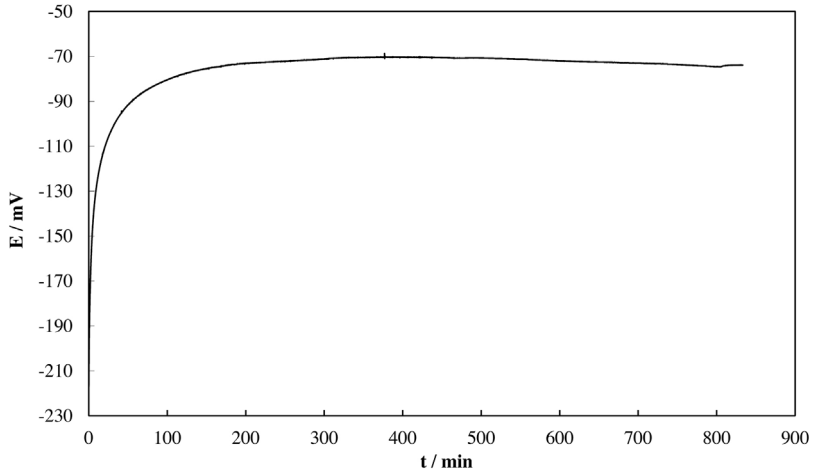

Fig. 2. OCP of an ND-Au screen-printed electrode during self-assembling process of 10 μL of 10.0 μmol L^{-1} aptamer.

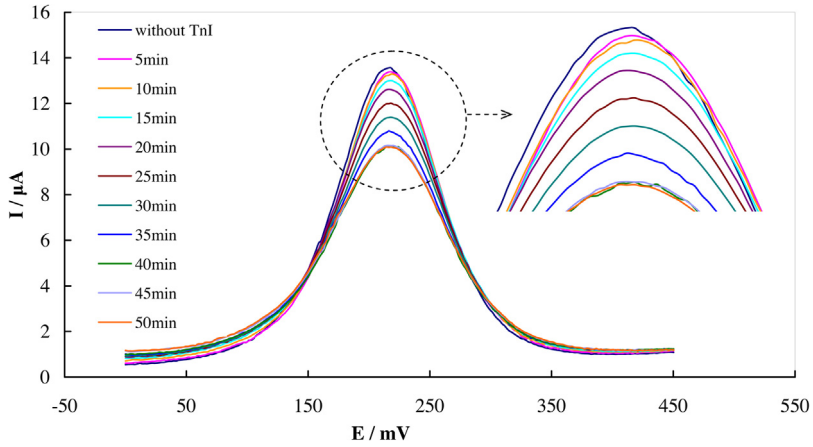

Fig. 3. DPVs of ferro/ferricyanide recorded using the aptasensor in Tris before and after binding with TnI solution of 2 ng mL^{-1} at different incubation times at 37 °C.

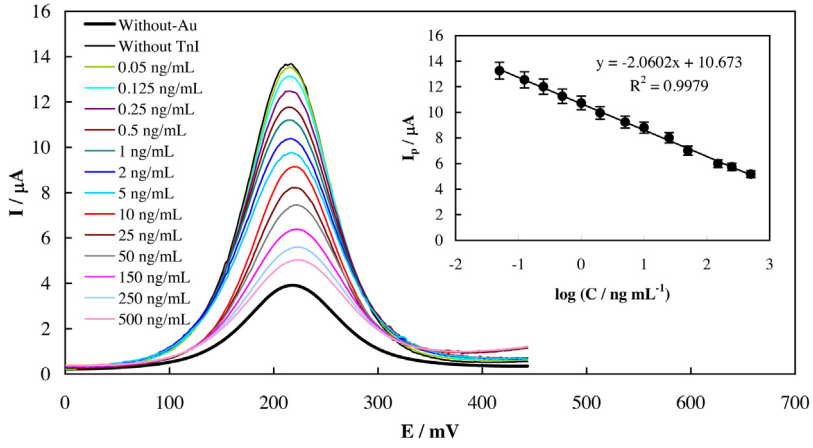

Fig. 4. DPVs of ferro/ferricyanide recorded using the aptasensor in Tris before (the upmost curve) and after binding with TnI of 0.05, 0.125, 0.25, 0.50, 1.0, 2.0, 5.0, 10, 25, 50, 150, 250 and 500 ng mL^{-1}, and a DPV of ferro/ferricyanide recorded using the Au/aptamer electrode in Tris before (the lowest curve) binding with TnI. Inset: Dependency of the peak currents in DPVs on the TnI concentration.

uniform morphology with high porosity providing a high surface area. The real surface area of the ND-Au electrode was electrochemically measured (Supplementary material S2). It was found that the Au and ND-Au electrodes had real surface areas of 0.035 and 0.26 cm^2, respectively, matching roughness factors of 1.11 and 7.51, respectively. This indicates that the nanodumbbells provide a high surface concentration of immobilized aptamer resulting in increment in the sensitivity of the aptasensor. The EDS spectrum is also confirmed the purity of the nanodumbbells. For nanodumbbells electrodeposition, a potential of 0 mV (vs. AgCl) was applied which is highly negative, compared to the formal potential of gold redox reaction (Au^{3+} + 3e- ¾ Au, E^0 = 1.27 V, vs. AgCl). This caused to a

Table 1
A comparison between different methods of TnI detection.

Detection method	Nanomaterial employed	Sensitivity[a]	Detection range	LOD	Ref.
Electrical immunosensing	Silicon nanowire	–	5 pg mL^{-1}–5 ng mL^{-1}	5 pg mL^{-1}	[19]
Electrochemical immunochip	–	0.62, 1.01 nA ng mL^{-1}	20 pg mL^{-1}–12.5 ng mL^{-1}	25 pg mL^{-1}	[20]
Electrochemical aptasensing [b]	Silica nanoparticles	0.05 μA (log (ng mL^{-1}))$^{-1}$[c]	1–10000 pmol L^{-1}	1.0 pmol L^{-1}	[31]
Electrochemical immunosensing	–	–	10–100 fg mL^{-1}	10 fg mL^{-1}	[47]
Electrochemical microchip	–	–	0.2 ng mL^{-1}–10 μg mL^{-1}	148 pg mL^{-1}	[48]
Electrochemical immunosensing	AuNPs	–	1–100 ng mL^{-1}	–	[49]
Electrochemical immunosensing	AuNPs	–	0.25–100 ng mL^{-1}	0.25 ng mL^{-1}	[50]
Electrochemical immunosensing	–	5.5 μA ng^{-1} mL	1–100 ng mL^{-1}	–	[51]
Electrochemical immunosensing	AuNPs	–	–	0.2 ng mL^{-1}	[52]
Surface plasmon resonance-based immunosensor	–	–	0–160 μg L^{-1}	68 ng L^{-1}	[53]
Electrochemiluminescence immunosensor	AuNPs	–	0.1–1000 ng mL^{-1}	0.06 ng mL^{-1}	[54]
Electrochemiluminescence immunosensor	AuNPs	–	0.1 pg mL^{-1}–0.2 ng mL^{-1}	12 fg mL^{-1}	[55]
Surface acoustic wave immunosensing	AuNPs	–	0.06-1.5 ng mL^{-1}	6.2 pg mL^{-1}	[56]
Electrochemical peptide-enabled biosensing	–	0.03 impedance μg^{-1} mL	0–10 μg mL^{-1}	0.34 μg mL^{-1}	[57]
Colorimetric immunosensing	AuNPs	–	0.01–5 ng mL^{-1}	0.01 ng mL^{-1}	[58]
Electrochemical molecularly imprinted polymer sensor	–	0.24 μA ng^{-1} mL	0.05-5.0 nM	0.027 nM	[59]
Field-effect transistors immunosensing	Silicon nanowire	–	0.092–46 ng mL^{-1}	0.092 ng mL^{-1}	[60]
Electrochemiluminescence immunosensor	AuNPs	–	2.5–10,000 pg mL^{-1}	2 pg mL^{-1}	[61]
Electrochemical immunosensing	Nanostructured tungsten trioxide	26.56 Ω ng^{-1} mL cm^2	1–250 ng mL^{-1}	16 ng mL^{-1}	[62]
Electrochemical immunosensing	Nanocomposites of AuNPs	4.01 μA ng^{-1} mL	0.05–3 ng mL^{-1}	0.05 ng mL^{-1}	[63]
Electrochemical peptide-enabled biosensing	AuNPs	9.34 Ω g^{-1} mL	15.5 pg mL^{-1}–1.55 ng mL^{-1}	3.4 pg mL^{-1}	[64]
Electrochemiluminescence peptide-enabled biosensing	AuNPs	–	3.0×10^{-12}–7.0×10^{-11} g mL^{-1}	0.5 pg mL^{-1}	[65]
Electrochemical immunosensing	Pt nanoparticles	80 Ω (log (ng mL^{-1}))$^{-1}$ cm^2	0.01–10 ng mL^{-1}	4.2 pg mL^{-1}	[66]
Electrochemical immunosensing	Graphene-multi walled carbon nanotubes	63.5 Ω (log (ng mL^{-1}))$^{-1}$ cm^2	0.001–10 ng mL^{-1}	0.94 pg mL^{-1}	[67]
Field-effect transistors immunosensing	ZnO nanoparticles	–	1 ng mL^{-1}–10 μg mL^{-1}	3.24 pg mL^{-1}	[68]
Electrochemical immunosensing	Au and Ag nanoparticles	91%	0.1–32 ng mL^{-1}	0.1 ng mL^{-1}	[69]
Electrochemical aptasensing [d]	Array of Au nanodumbbells	2.06 μA (log (ng mL^{-1}))$^{-1}$, 100%	0.05–500 ng mL^{-1}	8.0 pg mL^{-1} (0.36 pmol L^{-1})	This work

a. Values presented as physical quantities are calibration sensitivity, and values presented in percent are diagnostic sensitivity.
b. Aptamer sequences:
5′TCACACCCTCCCTCCCACATACCGCATACACTTTC TGATT3′
5′CCCGACCACGTCCCTGCCCTTTCCTAACCTGTTT GTTGAT3′
5′ATGCGTTGAACCCTCCTGACCGTTTATCACATACT CCAGA3′
5′CGTGCAGTACGCCAACCTTTCTCATGCGCTGCCC CTCTTA3′
5′CAACTGTAATGTACCCTCCTCGATCACGCACCACT TGCAT3′
5′CGCATGCCAAACGTTGCCTCATAGTTCCCTCCCC GTGTCC3′
c. The value was calculated from Fig. 3 in Reference [31].
d. Aptamer sequence:
5′ (SH)-(CH_2)6-AGTCTCCGCTGTCCTCCCGATGCACTTGACGTATGTCTCACTTTCTTTTCATTGACATGGGATGACGCCGTGACTG3&#x2032

rapid initial generation of a large number of gold nuclei (clusters and atoms) which was also accelerated by the Au electrode surface [44]. At the same time, putrescine (as an amine) was adsorbed on the surface of gold nuclei [45], while it born a net positive charge due to protonation of amine groups in the synthesis solution. Therefore, further adsorption of $AuCl_4^-$ ions occurred along the putrescine adsorbed plane.

3.2. Fabrication of the aptasensor

To optimize the immobilization time of the aptamer onto the ND-Au electrode surface, OCP of an ND-Au screen-printed electrode during the self-assembling process of 10 μL of 10.0 μmol L^{-1} aptamer at the surface was recorded at 4 °C and shown in Fig. 2. OCP changes showed continuous changes and reached a steady value after ~80 min. This indicates a dramatic attachment of the aptamer to the gold nanodumbbells surface, and this time was selected for the fabrication of the aptamer-immobilized gold electrodes.

In order to optimize the binding time of TnI to the aptamer at the aptasensor surface, DPVs were recorded using the aptasensor before and after binding with TnI solution of 2 ng mL^{-1} at different incubation times at 37 °C. The results are represented in Fig. 3. Based on the results (vide also infra), upon increment in the binding time, the peak current continuously decreased up to 40 min of binding time, and then reach to a stable value. Therefore, the maximum decrement in the peak current was observed for 40 min of binding, and this time was selected as the optimum binding time.

3.3. Evaluation of the aptasensor to detect TnI

Fig. 4 shows DPVs recorded using the aptasensor, before and after binding with various concentrations of TnI. The aptamer bears a net negative charge due to its phosphate-sugar back-

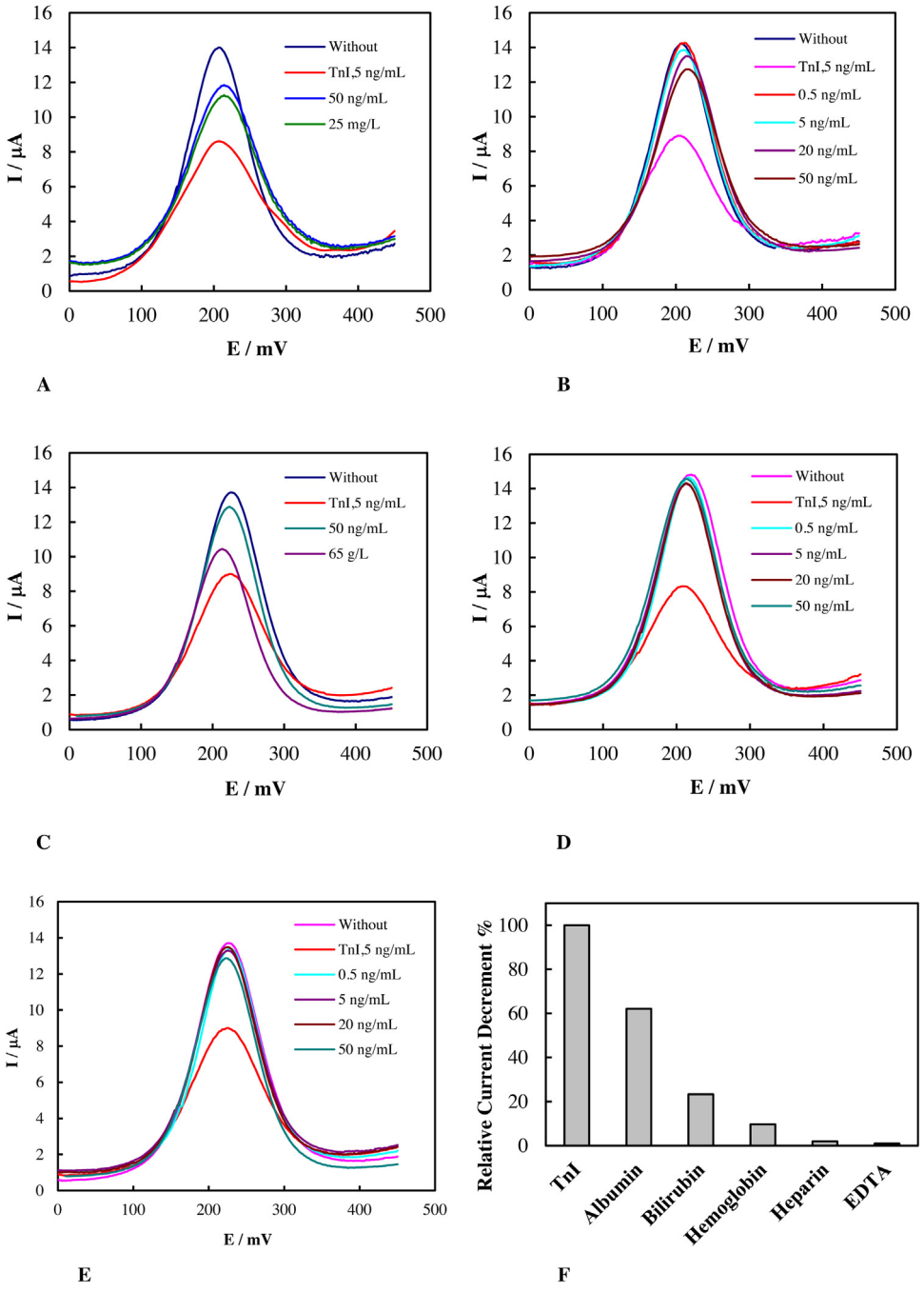

Fig. 5. DPVs of ferro/ferricyanide recorded using the aptasensor in Tris before (Without) and after its binding to 5.0 ng mL^{-1} TnI, and 50 ng mL^{-1} and 25 mg L^{-1} of bilirubin (A), 0.5, 5.0, 20, and 50 ng mL^{-1} of hemoglobin (B), 50 ng mL^{-1} and 65 g L^{-1} of human serum albumin (C), 0.5, 5.0, 20, and 50 ng mL^{-1} of heparin (D), and 0.5, 5.0, 20, and 50 ng mL^{-1} of EDTA (E). Changes in the peak currents for theses interferences as percentage of the 5.0 ng mL^{-1} TnI current (F).

bone. Therefore, ferro/ferricynaide ions have a certain approach to the aptamer surface and generate a certain peak current in DPVs. On the other hand, TnI also bears a net negative charge in the working pH due to its isoelectric point of 5.2-5.4 [46]. Therefore, TnI binding with the aptamer caused to an increment in the negative surface charge of the aptasensor; this increment was increased upon further increment in the TnI concentration and further repelling ferro/ferricynaide ions from the aptasensor surface. Hence, the aptasensor acts as a signal-off device. In the figure, a DPV of ferro/ferricyanide recorded using the Au/aptamer electrode in Tris before binding with TnI is also depicted. Comparing the peak currents in DPVs recorded for the Au/aptamer electrode and the aptasensor reveals that the nanodumbbells provided a larger surface area and a higher surface concentration of the aptamer. Dependency of the peak currents in DPVs recorded using the aptasensor for different concentrations of TnI presented in Fig. 4 on the TnI concentration is shown in Fig. 4, inset. The plot is linear in the range of 0.05–500 ng mL^{-1} of TnI with a regression equation of $y = -(2.0602 \pm 0.0282)x + (10.6731 \pm 0.0408)$. Based on the results, a limit of detection (LOD) for TnI was calculated with a corresponding signal equal to 3σ (σ is the standard deviation of the blank signal) and obtained as 8.0 pg mL^{-1}. In Scheme 1, fabrication of the aptasensor and TnI detection is presented. A comparison between different methods of TnI detection is also made in

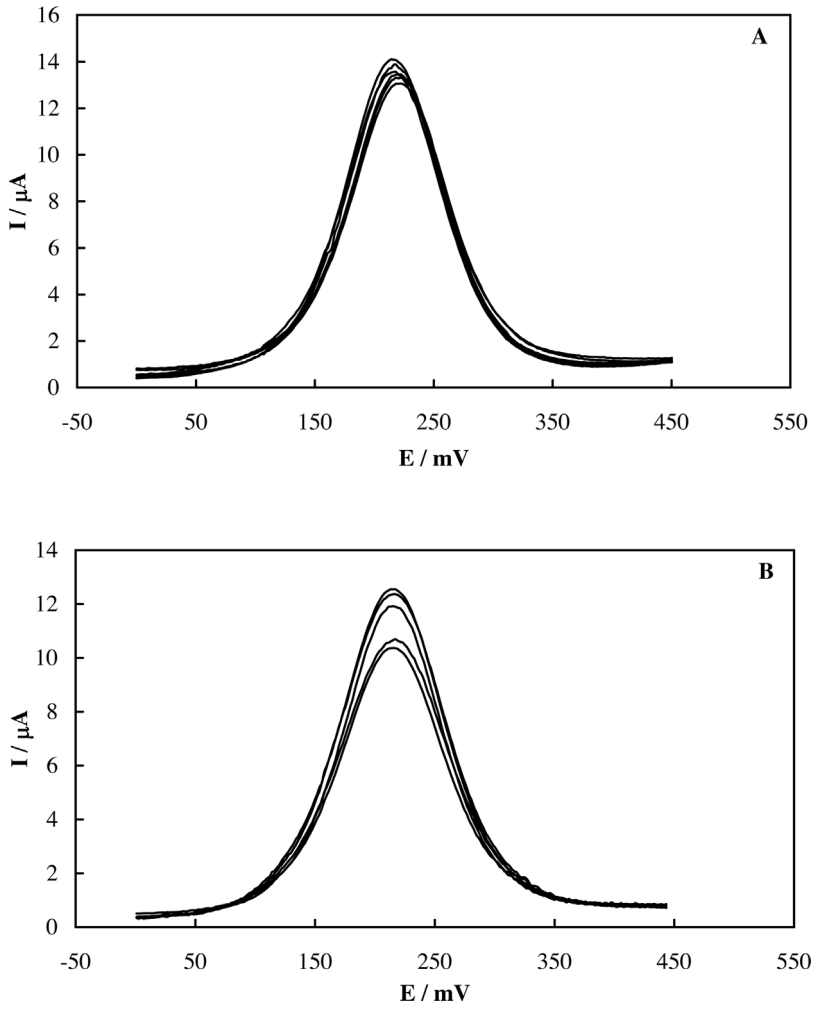

Fig. 6. DPVs of ferro/ferricyanide recorded using the aptasensor in Tris for the repeating fabrication cycles (A), and for rebinding with TnI (B). For the voltammograms in (A), after each fabrication, the aptasensor was washed by the Piranha solution and then re-fabricated (five times). For the voltammograms in (B), after binding the aptasensor with 1.0 ng mL^{-1} TnI, it was placed at 95 °C for 5 min, then rebind with the same concentration of TnI, and this cycle was repeated (five times).

Table 1. The aptasensor had better or comparable characteristics, and compare to the other aptamer-based TnI biosensor [31], it is fabricated more simple without using expensive transducer and redox marker, with higher sensitivity and lower LOD, based on a different aptamer.

In order to inspect the selectivity of the aptasensor, the interfering effect of human serum albumin, bilirubin, hemoglobin, heparin and ethylenediaminetetraacetic acid (EDTA) were evaluated. It should be noted that the highest levels of albumin is 5.5 g dL^{-1}, (total) bilirubin is 1.9 mg dL^{-1}, and hemoglobin is 18 g dL^{-1} in the blood. Heparin and EDTA are not naturally present in the serum samples, however, it is probable to add these species to the blood to obtain "plasma" samples. In addition, during serum sampling, hemoglobin settles and is not present in the serum, otherwise for inaccurate serum sampling. As for albumin interfering, due to the high difference between its molecular weight with TnI (~66 kDa for human serum albumin and ~23 kDa for TnI), the serum samples can be filtered by a typical ~40 kDa filter membrane to eliminate the albumin interfering. For quantitative evaluation, DPVs were recorded using the aptasensor after its binding to the interferences. Hemoglobin, heparin and EDTA were evaluated at four different concentrations of 0.5, 5.0, 20, and 50 ng mL^{-1}, human serum albumin at two concentrations of 50 ng mL^{-1} and 65 g L^{-1}, and bilirubin at two concentrations of 50 ng mL^{-1} and 25 mg L^{-1} were evaluated. The results are shown in Fig. 5(A–E). Changes in the peak currents for theses interferences as percentage of the 5.0 ng mL^{-1} TnI current are shown in Fig. 5(F). It should also be added that the different biologicals of enzymes, proteins, antibodies and hormones are present in the blood serum with high concentrations, and because the aptasensor was successfully applied for the analysis of TnI in the serum samples, (vide infra), the aptasensor was selective. In this regard, DPVs were recorded using the aptasensor after its binding to TnI, or TnI in the presence of HSA (Supplementary material S3). Based on the results, it seems that the interfering effect of this protein was decreased significantly in the presence of TnI.

3.4. Reproducibility, regeneration and stability of the aptasensor

After fabrication of the aptasensor, it was washed by the Piranha solution and then re-fabricated, and repeat this cycle five times to evaluate the fabrication reproducibility of the aptasensor. During the cycles, DPVs for the aptasensor were recorded and shown in Fig. 6A. In these DPVs, change in the peak current was inconsiderable with a relative standard deviation (RSD) of 3.9%.

After binding the aptasensor with a TnI concentration of 1.0 ng mL^{-1}, it was placed at 95 °C for 5 min to release the bound TnI. Then the aptasensor was rebind with the same concentration of TnI, and this cycle was repeated five times. During these cycles,

Table 2
TnI level (ng mL^{-1}) in human samples determined by ELISA and the aptasensor.

Sample Number	TnI levels-ELISA	TnI levels-Aptasensor
Negative samples-Negative results		
1	0.2	0.26
2	0.4	0.38
3	0.2	0.16
4	0.2	0.14
5	0.3	0.41
6	0.3	0.49
7	0.1	0.24
8	0.2	0.20
9	0.1	0.04
10	0.2	0.22
11	0	0.01
12	0.1	0.08
13	0.4	0.38
14	0.2	0.37
15	0.2	0.12
16	0.3	0.29
17	0	0
18	0	0.02
19	0	0.03
20	0.4	0.24
21	0.48	0.20
22	0	0.02
Negative samples-Positive results (false positive)		
23	**0.3**	**0.57**
24	**0.4**	**0.56**
25	**0.2**	**0.72**
26	**0.2**	**0.64**
Positive samples-Positive results		
27	1	0.88
28	0.7	0.90
29	0.5	0.55
30	8.4	11.63
31	1.1	1.25
32	0.5	0.64
33	0.8	1.06
34	0.5	0.51
35	4.3	4.13
36	1.2	1.07
37	0.8	0.98
38	0.6	0.95
39	9.4	4.91
40	1.1	1.76
41	1	1.72
42	0.5	0.75
43	5.6	4.12
44	1.3	1.14
45	3.2	3.46
46	11.8	8.85
47	8.6	7.54
48	73.7	65.9
49	5.1	24.5
50	14	8.68
51	3.2	4.10
52	28.7	17.2
53	6.5	8.45
54	24.7	19.1
55	9.5	18.6
56	4.6	1.84
57	9.8	17.7
58	3	5.04
59	5	3.90
60	0.9	0.51
61	1.1	1.41
62	53.9	16.3
63	16.3	10.5
64	15.4	20.8
65	2.1	4.28
66	38.9	27.9
67	14.9	18.0
68	2.9	3.60
69	68.7	48.0
70	31.8	31.8
71	84.8	82.7
72	84.4	71.9
73	68.7	51.3
74	2	2.20
75	1.4	2.24
76	12.6	8.25
77	55	57.9
78	35.4	41.6
79	49.8	40.6
80	12.9	22.6
81	9.6	15.2
82	21.3	24.5
83	32.1	31.9
84	11.7	20.4
85	41.4	44.1
86	6.0	9.60
87	10.7	18.8
88	3.0	1.98
89	29.2	30.7

DPVs were recorded and shown in Fig. 6B. The relative change in the peak current differences for the regeneration had a RSD of 12.0%.

The aptasensor was bound with a TnI concentration of 1.0 ng mL^{-1}, and then DPVs were recorded in consecutive days, while it was stored in Tris at 4 °C. It was found that the aptasensor signal slowly decreased, and reach to 85% of the initial value after 6 days. Therefore, 5 days was considered as the stability time of the aptasensor.

3.5. Applications of the aptasensor in early detection of AMI

In order to employ the aptasensor for the detection of AMI in human, blood serum samples of healthy persons and patients were firstly analyzed by the ELISA kit. Then, DPVs were recorded for all the samples. The obtained quantitative results for the TnI levels in all the samples determined by ELISA and the aptasensor are presented in Table 2. The results indicated that in the 89 samples, there were 4 false positive results with no false negative ones. Therefore, the aptasensor had a diagnostic sensitivity of 100% and a diagnostic specificity of 85%.

4. Conclusion

Due to the importance of detection of TnI biomarker in the diagnosis, prevention and treatment of AMIs, fabrication of a TnI sensor is an important achievement in health policies and preventing deaths caused by AMIs. Here, an array of gold nanodumbbells which was simply fabricated was applied to design an electrochemical TnI aptasensor indicating a successful typical application of chemistry, medicine and nanotechnology in the advanced and fast diagnosis of AMIs. This TnI aptasensor had high detection ability with low cost without using any tag or label, and can be used as an alternative to other conventional diagnostic methods for clinical analysis of AMIs.

Acknowledgments

The paper has been extracted from the M. Negahdary PhD thesis supported by the Research Council of Shahid Sadoughi University of Medical Sciences (4350), Shiraz University of Medical Sciences (9665) and Nanomedicine and Nanobiology Research Center, Iran.

Appendix A. Supplementary data

Supplementary data associated with this article can be found, in the online version, at http://dx.doi.org/10.1016/j.snb.2017.05.149.

References

[1] D.P. Mann, P. Zipes, Braunwald's Heart Disease: a Textbook of Cardiovascular Medicine, Elsevier Health Sciences, 2014.
[2] H. El Aidi, A. Adams, K.G. Moons, H.M. Den Ruijter, P.T.M. Willem, P.A. Doevendans, E. Nagel, S. Schalla, M.L. Bots, T. Leiner, Cardiac magnetic resonance imaging findings and the risk of cardiovascular events in patients with recent myocardial infarction or suspected or known coronary artery disease: a systematic review of prognostic studies, J. Am. Coll. Cardiol. 63 (2014) 1031–1045.
[3] M.M. Demidova, A. Martin-Yebra, J.P. Martinez, V. Monasterio, S. Koul, J. van der Pals, D. Romero, P. Laguna, D. Erlinge, P.G. Platonov, T wave alternans in experimental myocardial infarction: time course and predictive value for the assessment of myocardial damage, J. Electrocardiol. 46 (2013) 263–269.
[4] Q.A. Acton. Heart Attack, New Insights for the Healthcare Professional, 2013, 2013 Edition: Scholarly Editions.
[5] K.K. Stout, Adult Congenital Heart Disease: The Coming Tide, Cardiology Clinics, Elsevier Health Sciences, 2016.
[6] P. Prandoni, Venous and arterial thrombosis: is there a link? Adv. Exp. Med. Biol. 906 (2017) 273–283.
[7] G.S. Bodor, Biochemical markers of myocardial damage, Ejifcc 27 (2016) 95–111.
[8] A.B. Storrow, R.M. Nowak, D.B. Diercks, A.J. Singer, A.H. Wu, E. Kulstad, F. LoVecchio, C. Fromm, G. Headden, T. Potis, C.J. Hogan, J.W. Schrock, D.P. Zelinski, M.R. Greenberg, R.H. Christenson, J.C. Ritchie, J.S. Chamberlin, K.R. Bray, D.W. Rhodes, D. Trainor, P.C. Southwick, Absolute and relative changes (delta) in troponin I for early diagnosis of myocardial infarction: results of a prospective multicenter trial, Clin. Biochem. 48 (2015) 260–267.
[9] N. Wettersten, A.S. Maisel, Biomarkers for heart failure: an update for practitioners of internal medicine, Am. J. Med. 129 (2016) 560–567.
[10] A.S. Jaffe, R.S. Wright, High-sensitivity cardiac troponin and primary prevention: an important new role, J. Am. Coll. Cardiol. 68 (2016) 2729–2732.
[11] J.E. Zamora, M. Papadaki, A.E. Messer, S.B. Marston, I.R. Gould, Troponin structure: its modulation by Ca(2+) and phosphorylation studied by molecular dynamics simulations, Phys. Chem. Chem. Phys. 18 (2016) 20691–20707.
[12] J.R. Tate, D.M. Bunk, R.H. Christenson, A. Katrukha, J.E. Noble, R.A. Porter, H. Schimmel, L. Wang, M. Panteghini, Standardisation of cardiac troponin I measurement: past and present, Pathology 42 (2010) 402–408.
[13] A.A. Mohammed, J.L. Januzzi Jr., Clinical applications of highly sensitive troponin assays, Cardiol. Rev. 18 (2010) 12–19.
[14] A. Bini, S. Centi, S. Tombelli, M. Minunni, M. Mascini, Development of an optical RNA-based aptasensor for C-reactive protein, Anal. Bioanal. Chem. 390 (2008) 1077–1086.
[15] S.A. Vance, M.G. Sandros, Zeptomole detection of C-reactive protein in serum by a nanoparticle amplified surface plasmon resonance imaging aptasensor, Sci. Rep. 4 (2014) 5129.
[16] A. Qureshi, Y. Gurbuz, S. Kallempudi, J.H. Niazi, Label-free RNA aptamer-based capacitive biosensor for the detection of C-reactive protein, Phys. Chem. Chem. Phys. 12 (2010) 9176–9182.
[17] L. Mao, R. Yuan, Y. Chai, Y. Zhuo, Y. Xiang, Signal-enhancer molecules encapsulated liposome as a valuable sensing and amplification platform combining the aptasensor for ultrasensitive ECL immunoassay, Biosens. Bioelectron. 26 (2011) 4204–4208.
[18] X.-H. Lai, R.-L. Liang, T.-C. Liu, Z.-N. Dong, Y.-S. Wu, L.-H. Li, A fluorescence immunochromatographic assay using europium (III) chelate microparticles for rapid, quantitative and sensitive detection of creatine kinase MB, J. Fluoresc. 26 (2016) 987–996.
[19] K. Kim, C. Park, D. Kwon, D. Kim, M. Meyyappan, S. Jeon, J.-S. Lee, Silicon nanowire biosensors for detection of cardiac troponin I (cTnI) with high sensitivity, Biosens. Bioelectron. 77 (2016) 695–701.
[20] J. Horak, C. Dincer, E. Qelibari, H. Bakirci, G. Urban, Polymer-modified microfluidic immunochip for enhanced electrochemical detection of troponin I, Sens. Actuators B 209 (2015) 478–485.
[21] S.-W. Kim, I.-H. Cho, J.-N. Park, S.-M. Seo, S.-H. Paek, A high-performance fluorescence immunoassay based on the relaxation of quenching, exemplified by detection of cardiac troponin I, Sensors 16 (2016) 669.
[22] M. Shan, M. Li, X. Qiu, H. Qi, Q. Gao, C. Zhang, Sensitive electrogenerated chemiluminescence peptide-based biosensor for the determination of troponin I with gold nanoparticles amplification, Gold Bull. 47 (2014) 57–64.
[23] C. Wang, H. Qi, X. Qiu, Q. Gao, C. Zhang, Homogeneous electrogenerated chemiluminescence peptide-based method for determination of troponin I, Anal. Methods 4 (2012) 2469–2474.
[24] Y. Zhou, Y. Zhuo, N. Liao, Y. Chai, R. Yuan, Ultrasensitive electrochemiluminescent detection of cardiac troponin I based on a self-enhanced Ru(II) complex, Talanta 129 (2014) 219–226.
[25] W.-J. Kim, H.Y. Cho, B.K. Kim, C. Huh, K.H. Chung, C.-G. Ahn, Y. Jun. Kima, A. Kim, Highly sensitive detection of cardiac troponin I in human serum using gold nanoparticle-based enhanced sandwich immunoassay, Sens. Actuators B 221 (2015) 537–543.
[26] T. Keller, T. Zeller, D. Peetz, S. Tzikas, A. Roth, E. Czyz, C. Bickel, S. Baldus, A. Warnholtz, M. Fröhlich, C.R. Sinning, M.S. Eleftheriadis, P.S. Wild, R.B. Schnabel, E. Lubos, N. Jachmann, S. Genth-Zotz, F. Post, V. Nicaud, L. Tiret, K.J. Lackner, T.F. Münzel, S. Blankenberg, Sensitive troponin I assay in early diagnosis of acute myocardial infarction, N. Engl. J. Med. 361 (2009) 868–877.
[27] A. Rahi, N. Sattarahmady, H. Heli, Label-free electrochemical aptasensing of the human prostate-specific antigen using gold nanospears, Talanta 156–157 (2016) 218–224.
[28] S.G. Meirinho, L.G. Dias, A.M. Peres, L.R. Rodrigues, Voltammetric aptasensors for protein disease biomarkers detection: a review, Biotechnol. Adv. 34 (2016) 941–953.
[29] X. Yang, Y. Wang, K. Wang, Q. Wang, P. Wang, M. Lin, N. Chena, Y. Tana, DNA aptamer-based surface plasmon resonance sensing of human C-reactive protein, RSC Adv. 4 (2014) 30934–30937.
[30] M.-C. Lin, J. Nawarak, T.-Y. Chen, H.-Y. Tsai, J.-F. Hsieh, S. Sinchaikul, S.-T. Chen, Rapid detection of natriuretic peptides by a microfluidic LabChip analyzer with DNA aptamers: application of natriuretic peptide detection, Biomicrofluidics 3 (2009) 034101.
[31] H. Jo, H. Gu, W. Jeon, H. Youn, J. Her, S.-K. Kim, J. Lee, J.H. Shin, C. Ban, Electrochemical aptasensor of cardiac troponin I for the early diagnosis of acute myocardial infarction, Anal. Chem. 87 (2015) 9869–9875.
[32] D. Proske, M. Blank, R. Buhmann, A. Resch, Aptamers-basic research, drug development, and clinical applications, Appl. Microbiol. Biotechnol. 69 (2005) 367–374.
[33] A. Rahi, K. Karimian, H. Heli, Nanostructured materials in electroanalysis of pharmaceuticals, Anal. Biochem. 497 (2016) 39–47.
[34] M. Moradi, N. Sattarahmady, A. Rahi, G. Hatam, S.R. Sorkhabadi, H. Heli, A label-free, PCR-free and signal-on electrochemical DNA biosensor for Leishmania major based on gold nanoleaves, Talanta 161 (2016) 48–53.
[35] A. Rahi, N. Sattarahmady, H. Heli, Zepto-molar electrochemical detection of Brucella genome based on gold nanoribbons covered by gold nanoblooms, Sci. Rep. 5 (2015) 18060.
[36] A. Rahi, N. Sattarahmady, H. Heli, An ultrasensitive electrochemical genosensor for Brucella based on palladium nanoparticles, Anal. Biochem. 510 (2016) 11–17.
[37] I. Palchetti, M. Mascini, Electrochemical nanomaterial-based nucleic acid aptasensors, Anal. Bioanal. Chem. 402 (2012) 3103–3114.
[38] R. Sharma, K. Ragavan, M. Thakur, K. Raghavarao, Recent advances in nanoparticle based aptasensors for food contaminants, Biosens. Bioelectron. 74 (2015) 612–627.
[39] Y. Lim, A. Kouzani, W. Duan, Aptasensors: a review, J. Biomed. Nanotechnol. 6 (2010) 93–105.
[40] P. Hong, W. Li, J. Li, Applications of aptasensors in clinical diagnostics, Sensors 12 (2012) 1181–1193.
[41] A.B. Iliuk, L. Hu, W.A. Tao, Aptamer in bioanalytical applications, Anal. Chem. 83 (2011) 4440–4452.
[42] L. Wang, X. Chen, X. Wang, X. Han, S. Liu, C. Zhao, Electrochemical synthesis of gold nanostructure modified electrode and its development in electrochemical DNA biosensor, Biosens. Bioelectron. 1 (2011) 151–157.
[43] M. Moradi, N. Sattarahmady, G.R. Hatam, H. Heli, Electrochemical genosensing of leishmania major using gold hierarchical nanoleaflets, J. Biol. Today's World 5 (2016) 128–136.
[44] J. Wang, G. Duan, Y. Li, G. Liu, Z. Dai, H. Zhang, W. Cai, An invisible template method toward gold regular arrays of nanoflowers by electrodeposition, Langmuir 29 (2013) 3512–3517.
[45] Y. Bu, S.J. Park, S.W. Lee, Diamine-linked array of metal (Au, Ag) nanoparticles on glass substrates for reliable surface-enhanced Raman scattering (SERS) measurements, Curr. Appl. Phys. 14 (2014) 784–789.
[46] E. Peronnet, L. Becquart, J. Martinez, J.-P. Charrier, C. Jolivet-Reynaud, Isoelectric point determination of cardiac troponin I forms present in plasma from patients with myocardial infarction, Clin. Chim. Acta 377 (2007) 243–247.
[47] M.R. Akanda, M.A. Aziz, K. Jo, V. Tamilavan, M.H. Hyun, S. Kim, H. Yang, Optimization of phosphatase-and redox cycling-based immunosensors and its application to ultrasensitive detection of troponin I, Anal. Chem. 83 (2011) 3926–3933.
[48] S. Ko, B. Kim, S.-S. Jo, S.Y. Oh, J.-K. Park, Electrochemical detection of cardiac troponin I using a microchip with the surface-functionalized poly (dimethylsiloxane) channel, Biosens. Bioelectron. 23 (2007) 51–59.
[49] A.S. Ahammad, Y.-H. Choi, K. Koh, J.-H. Kim, J.-J. Lee, M. Lee, Electrochemical detection of cardiac biomarker troponin I at gold nanoparticle-modified ITO electrode by using open circuit potential, Int. J. Electrochem. Sci. 6 (2011) 1906–1916.
[50] A. Periyakaruppan, R.P. Gandhiraman, M. Meyyappan, J.E. Koehne, Label-free detection of cardiac troponin-I using carbon nanofiber based nanoelectrode arrays, Anal. Chem. 85 (2013) 3858–3863.
[51] K.K. Jagadeesan, S. Kumar, G. Sumana, Application of conducting paper for selective detection of troponin, Electrochem. Commun. 20 (2012) 71–74.
[52] V. Bhalla, S. Carrara, P. Sharma, Y. Nangia, C.R. Suri, Gold nanoparticles mediated label-free capacitance detection of cardiac troponin I, Sens. Actuators B 161 (2012) 761–768.
[53] Y.-C. Kwon, M.-G. Kim, E.-M. Kim, Y.-B. Shin, S.-K. Lee, S.D. Lee, M-Je. Cho, H-Su. Ro, Development of a surface plasmon resonance-based immunosensor for the rapid detection of cardiac troponin I, Biotechnol. Lett. 33 (2011) 921–927.
[54] F. Li, Y. Yu, H. Cui, D. Yang, Z. Bian, Label-free electrochemiluminescence immunosensor for cardiac troponin I using luminol functionalized gold nanoparticles as a sensing platform, Analyst 138 (2013) 1844–1850.
[55] L. Zhang, C. Xiong, H. Wang, R. Yuan, Y. Chai, A sensitive electrochemiluminescence immunosensor for cardiac troponin I detection

based on dual quenching of the self-enhanced Ru(II) complex by folic acid and in situ generated oxygen, Sens. Actuators B 241 (2017) 765–772.
[56] J. Lee, Y. Lee, J.-Y. Park, H. Seo, T. Lee, W. Lee, S.K. Kima, Y.K. Hahna, J. Junga, S. Kimb, Y.-S. Choia, S.S. Leea, Sensitive and reproducible detection of cardiac troponin I in human plasma using a surface acoustic wave immunosensor, Sens. Actuators B 178 (2013) 19–25.
[57] J. Wu, D.M. Cropek, A.C. West, S. Banta, Development of a troponin I biosensor using a peptide obtained through phage display, Anal. Chem. 82 (2010) 8235–8243.
[58] W.-Y. Wu, Z.-P. Bian, W. Wang, J.-J. Zhu, PDMS gold nanoparticle composite film-based silver enhanced colorimetric detection of cardiac troponin I, Sens. Actuators B 147 (2010) 298–303.
[59] J. Zuo, X. Zhao, X. Ju, S. Qiu, W. Hu, T. Fan, J. Zhang, A new molecularly imprinted polymer (MIP)-based electrochemical sensor for monitoring cardiac troponin I (cTnI) in the serum, Electroanalysis 28 (2016) 2044–2049.
[60] T. Kong, R. Su, B. Zhang, Q. Zhang, G. Cheng, CMOS-compatible, label-free silicon-nanowire biosensors to detect cardiac troponin I for acute myocardial infarction diagnosis, Biosens. Bioelectron. 34 (2012) 267–272.
[61] W. Shen, D. Tian, H. Cui, D. Yang, Z. Bian, Nanoparticle-based electrochemiluminescence immunosensor with enhanced sensitivity for cardiac troponin I using N-(aminobutyl)-N-(ethylisoluminol)-functionalized gold nanoparticles as labels, Biosens. Bioelectron. 27 (2011) 18–24.
[62] D. Sandil, S. Kumar, K. Arora, S. Srivastava, B. Malhotra, S. Sharma, N.K. Puri, Biofunctionalized nanostructured tungsten trioxide based sensor for cardiac biomarker detection, Mater. Lett. 186 (2017) 202–205.
[63] G. Liu, M. Qi, Y. Zhang, C. Cao, E.M. Goldys, Nanocomposites of gold nanoparticles and graphene oxide towards an stable label-free electrochemical immunosensor for detection of cardiac marker troponin-I, Anal. Chim. Acta 909 (2016) 1–8.
[64] B. Wang, R. Jing, H. Qi, Q. Gao, C. Zhang, Label-free electrochemical impedance peptide-based biosensor for the detection of cardiac troponin I incorporating gold nanoparticles modified carbon electrode, J. Electroanal. Chem. 781 (2016) 212–217.
[65] M. Dong, M. Li, H. Qi, Z. Li, Q. Gao, C. Zhang, Electrogenerated chemiluminescence peptide-based biosensing method for cardiac troponin I using peptide-integrating Ru (bpy) 3 2+-functionalized gold nanoparticles as nanoprobe, Gold Bull. 48 (2015) 21–29.
[66] S. Singal, A.K. Srivastava, A.M. Biradar, A. Mulchandani, Pt nanoparticles-chemical vapor deposited graphene composite based immunosensor for the detection of human cardiac troponin I, Sens. Actuators B 205 (2014) 363–370.
[67] S. Singal, A.K. Srivastava, S. Dhakate, A.M. Biradar, Electroactive graphene-multi-walled carbon nanotube hybrid supported impedimetric immunosensor for the detection of human cardiac troponin-I, RSC Adv. 5 (2015) 74994–75003.
[68] M.F.M. Fathil, M.K. Md Arshad, A.R. Ruslinda, S.C.B. Gopinath, M. Nuzaihan, M.N.R. Adzhri, U. Hashima, H.Y. Lamd, Substrate-gate coupling in ZnO-FET biosensor for cardiac troponin I detection, Sens. Actuators B 242 (2017) 1142–1154.
[69] A.A. Shumkov, E.V. Suprun, S.Z. Shatinina, A.V. Lisitsa, V.V. Shumyantseva, A.I. Archakov, Gold and silver nanoparticles for electrochemical detection of cardiac troponin I based on stripping voltammetry, BioNanoScience 3 (2013) 216–222.

Biographies

M. Negahdary received his MSc. in biochemistry from Payame Noor University, Tehran, Iran at 2011. He is a PhD candidate in Yazd Cardiovascular Research Center. His interests include biosensors, nanobiology and nanomedicine.

Dr. Mostafa Behjati-Ardakani received his MD in pediatric cardiology from Iran University of Medical Sciences at 1997. He now is a professor and faculty member at Shahid Sadoughi University of Medical Sciences, Yazd Iran with interesting in congenital heart diseases.

Dr. N. Sattarahmady received her Ph.D. in biophysics from Institute of Biochemistry and Biophysics, University of Tehran, Iran. She currently is an associate professor of biophysics at Shiraz University of Medical Sciences. Her current interests include protein structure, design of nanostructured materials for encapsulation, drug delivery and biosensors, and nanomedicine.

Dr. H. Yadegari received his Ph.D. in Materials Engineering from University of Western Ontario. He is currently a postdoctoral fellow at the University of Western Ontario. His main research interests are associated with energy conversion and storage, electrochemistry of nanomaterials and electrocatalysis.

Dr. H. Heli received his PhD in electrochemistry from K.N. Toosi University of Technology, Tehran, Iran. He currently is an assistant professor of chemistry at Shiraz University of Medical Sciences, Shiraz, Iran. His major interests are synthesis of new nanostructured and targeted materials and their applications in medical nanodevices.